

Recurrence of large paleo-earthquakes in Kashmir Himalaya seismic gap (Riasi area, India)

Riccardo Vassallo^{a,*}, Jean-Louis Mugnier^a, Hervé Jomard^b, Joaquin Cortès Aranda^{a,c}, Manzoor A. Malik^d, François Jouanne^a, Jean-François Buoncristiani^e

^a Université Grenoble Alpes, Université Savoie Mont Blanc, CNRS, ISTERre, IFFSTAR, 38000 Grenoble, France

^b Institut de Radioprotection et de Sécurité Nucléaire, Fontenay-aux-Roses, France

^c Universidad de Concepción, Departamento de Ciencias de la Tierra, Concepción, Chile

^d Department of Geology, University of Jammu, India

^e Biogéosciences, UMR 6282 CNRS/université Bourgogne Franche-Comté, Dijon, France

ARTICLE INFO

Keywords:

Himalaya
Fault
Paleoseismicity
Ruptures
Seismic hazard

ABSTRACT

In Kashmir Himalaya, the Medicott-Wadia Thrust is a main active fault responsible for the crustal accretionary prism building during the Late Quaternary. Because of the long seismic silence during the last five centuries, it is a key structure to be studied in order to estimate the regional seismic hazard. In the Riasi area, the analysis of two paleoseismological trenches allowed us identifying and measuring several seismic ruptures over the last ~3500 years. We determined that the oldest rupture occurred around 1600–1000 BC, while the youngest occurred after 1470 AD. The latest event is compatible with the great 1555 AD ($M_w > 7.5$) Kashmir earthquake, whose evidence at the surface had not yet been recognized. Our results show that despite the long-lasting seismic gap, the Medicott-Wadia Thrust is a main seismogenic structure in the region, able to produce large earthquakes. Their recurrence interval ranges between 500 and 700 years, implying that a main seismic event could occur in the next decades. These seismic ruptures are localized over gently-dipping fault branches associated with decameter-scale scarps. The morphologies observed are due to a significant non-localized component of the deformation in Quaternary sediments.

1. Introduction

Seismicity over the past two centuries indicates that North-western Himalaya is one of the most active regions of the whole collisional belt. This part of the Himalayan arc has been struck by two major earthquakes a hundred years apart: the 1905 Kangra M_w 7.8 event (Bilham, 2001; Ambraseys and Douglas, 2004; Wallace et al., 2005) and the 2005 Balakhot-Bagh M_w 7.6 event (Avouac et al., 2006; Kumahara and Nakata, 2006; Pathier et al., 2006; Kaneda et al., 2008; Kondo et al., 2008; Yan et al., 2013) (Fig. 1). However, in between these two coseismic rupture zones, a 200-km-long seismic gap has not registered any major earthquake during the last five centuries and no paleoseismological calendar associated with potential seismogenic structures in the area is available (Bilham, 2019).

The latest big seismic event in this area occurred in 1555 AD, when a $M_w > 7.5$ earthquake shook the Kashmir basin and its surroundings (Ambraseys and Jackson, 2003; Ambraseys and Douglas, 2004). The fault that ruptured during this event is still unknown due to the poor

accuracy of historical archives and the absence of paleoseismological studies in the region. Concerning the potential source of such an earthquake, Bilham (2019) mentions its possible occurrence along several identified fault systems located either south or north of the Pir-Panjial range (Fig. 1). In the former case, the main candidates are the Main Frontal Thrust (MFT) and the Medicott-Wadia Thrust (MWT), also called the Riasi Thrust (Vassallo et al., 2015; Gavillot et al., 2016; Mugnier et al., 2017). In the latter case, the principal fault observed is the Balapur Thrust (BT) (Ahmad and Bhat, 2012), then mapped through the whole Kashmir Basin and thus renamed the Kashmir Basin Fault (KBF) (Shah, 2013, 2015). This uncertainty highlights the lack of crucial paleoseismological evidences for a more robust regional seismic hazard assessment.

Most of the shortening across Kashmir Himalaya is due to India-Eurasia convergence, as inferred from geodetic studies (~1.4 cm/yr) (Schiffman et al., 2013; Jade et al., 2014). It is mainly accommodated by two active thrusts: the MFT and the MWT (Vassallo et al., 2015; Gavillot et al., 2016) (Fig. 1). A smaller amount of the deformation is

* Corresponding author.

E-mail address: rvass@univ-smb.fr (R. Vassallo).

<https://doi.org/10.1016/j.jseaes.2020.104505>

Received 1 October 2019; Received in revised form 20 July 2020; Accepted 24 July 2020

Available online 30 July 2020

1367-9120/© 2020 Elsevier Ltd. All rights reserved.

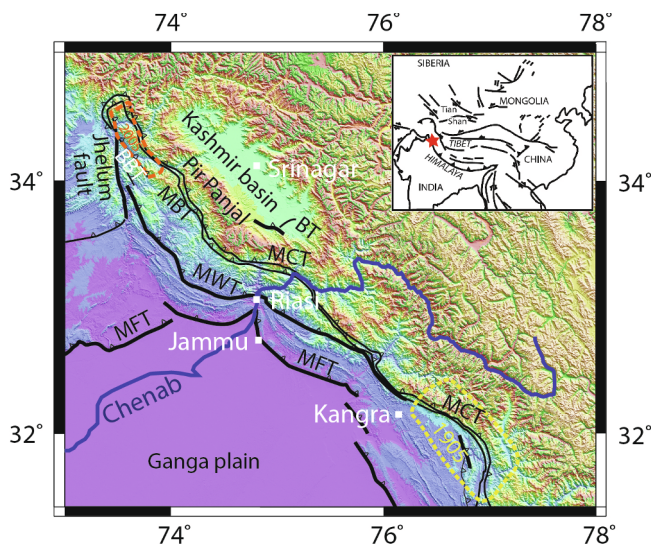


Fig. 1. Morpho-structural map of north-western Himalaya with main Cenozoic faults. Active thrusts are shown using bold lines. MFT: Main Frontal Thrust; MWT: Medlicott-Wadia Thrust; MBT: Main Boundary Thrust; MCT: Main Central Thrust; BBT: Balakhot-Bagh Thrust; BT: Balapur Thrust. Inferred rupture area for the 1905 earthquake (Wallace et al., 2005) and estimated rupture area for the 2005 earthquake (Avouac et al., 2006) are shown using dotted lines. In the box: the star indicates the localization of the study area at the continental scale.



Fig. 2. Faults map of the MWT system in the Riasi reentrant over a SPOT5 satellite image.

distributed on shorter and more internal thrusts. Among them, within the Kashmir Basin, the BT or KBF is thought to be the most active structure (Ahmad and Bhat, 2012; Shah, 2013) (Fig. 1). However, the geometry and kinematics of these faults are matter of discussion (Dar et al., 2014; Shah, 2016) and the deformation rates that they accommodate are unknown. While the MFT in Jammu region is a blind structure, and cannot be directly studied in terms of paleoseismicity, the MWT is an out-of-sequence structure reaching the surface and deforming Quaternary markers (Thakur et al., 2010; Mugnier et al., 2017). Along the mountain front, local scarps of several tens or hundreds of meters are developed where this fault affects the Quaternary

surfaces. The most outstanding geomorphic expression of MWT is observed in the Riasi area, therefore chosen for paleoseismological study (Figs. 2–4).

In this area, previous studies were focused on the regional active tectonics (Vassallo et al., 2015), the control of the sedimentation in the Riasi area (Vignon et al., 2017) and the tectonic pattern in the vicinity of Riasi (Gavillot et al., 2016; Mugnier et al., 2017). A long-term vertical throw rate across the MWT, based on the analysis of a hectometer-scale fault scarp, yields values between 0.9 and 1.3 cm/yr during the last 36 ka (Vignon et al., 2017). Considering that fault dip at depth is 45°, this result is consistent with the 1.1 ± 0.4 cm/yr shortening rate, inferred for the last 15 ka (Vassallo et al., 2015; Mugnier et al., 2017). Although a smaller rate estimate (0.6–0.7 cm/yr) in the same area was proposed by Gavillot et al. (2016), all these studies agree that Quaternary cumulative slip along the different Riasi Fault branches is in the order of several kilometers and that MWT is a major active fault in the Himalayan building process.

Therefore, the goal of our study is to complement this available dataset through paleoseismological investigations along the MWT. Our primary objectives are to determine and discuss the recurrence of surface rupturing earthquakes along this main structure of the Kashmir seismic gap zone and if possible to find the primary ruptures associated with the 1555 AD earthquake. Then, the chronology of paleo-earthquakes will be discussed in the light of the historical archives in order to propose a robust paleoseismic calendar. The geometry of both coseismic ruptures and fault scarps will be analyzed to better understand how deformation is expressed in this kind of tectonic context. These data are fundamental to characterize the seismic behavior of active faults and thus to better evaluate the related seismic hazard in such a densely populated region of Himalaya.

2. Tectonic and geological context

In the Kashmir Himalayan region, four main sub-parallel thrusts have been active during the Late Cenozoic (Nakata et al., 1991). From North to South – from the most internal to the most external fault – they are the Balapur Thrust (BT) or Kashmir Basin Fault (KBF) (Ahmad and Bhat, 2012; Shah, 2013), the Main Boundary Thrust (MBT) (Burbank et al., 1986), the Medlicott–Wadia Thrust (MWT) (Thakur et al., 2010), and the Main Frontal Thrust (MFT) (Powers et al., 1998) (Fig. 1). In the Kashmir Basin, the BT-KBF is a discontinuous thrust that deforms Quaternary deposits lying over the Higher Himalaya unit. On the southern side of the Pir Panjal range, the MBT makes the Lesser Himalaya unit thrust over the red sandstones of the Cenozoic Murree formation, that lies unconformably on a Precambrian stromatolites-rich limestone (Gansser, 1964). In the Riasi area, the MWT allows the Precambrian limestone to override the Late Cenozoic conglomerates and sandstones of the Siwaliks formation (Krishnaswamy et al., 1970; Hebel et al., 2010; Vignon, 2011). At the toes of the Himalayan range, the MFT is a blind ramp that is at the origin of a folding in the Siwaliks units with a ~20-km-wide wavelength.

The MBT ceased its activity in the region several tens of thousands of years ago, while the BT-KBF, the MWT and the MFT deform Late-Quaternary markers and are therefore considered as potentially seismogenic (Shah, 2013; Vassallo et al., 2015). We focused our study on the MWT, which is the thrust absorbing most of the regional shortening across the Himalayan belt (Vassallo et al., 2015; Gavillot et al., 2016).

3. Morphotectonic record in the Riasi area

The Riasi area is located at the toes of the main Himalayan relief (Figs. 2–4), where the Quaternary deposits belong to a kilometer-scale alluvial fan system deposited by the Nodda river, a small tributary of the Chenab river (Vignon et al., 2017). Morphologically, this fan displays an older surface S3 and a younger fill-and-cut terrace S2, inset in surface S3 and joining laterally the coeval fan of a southern stream

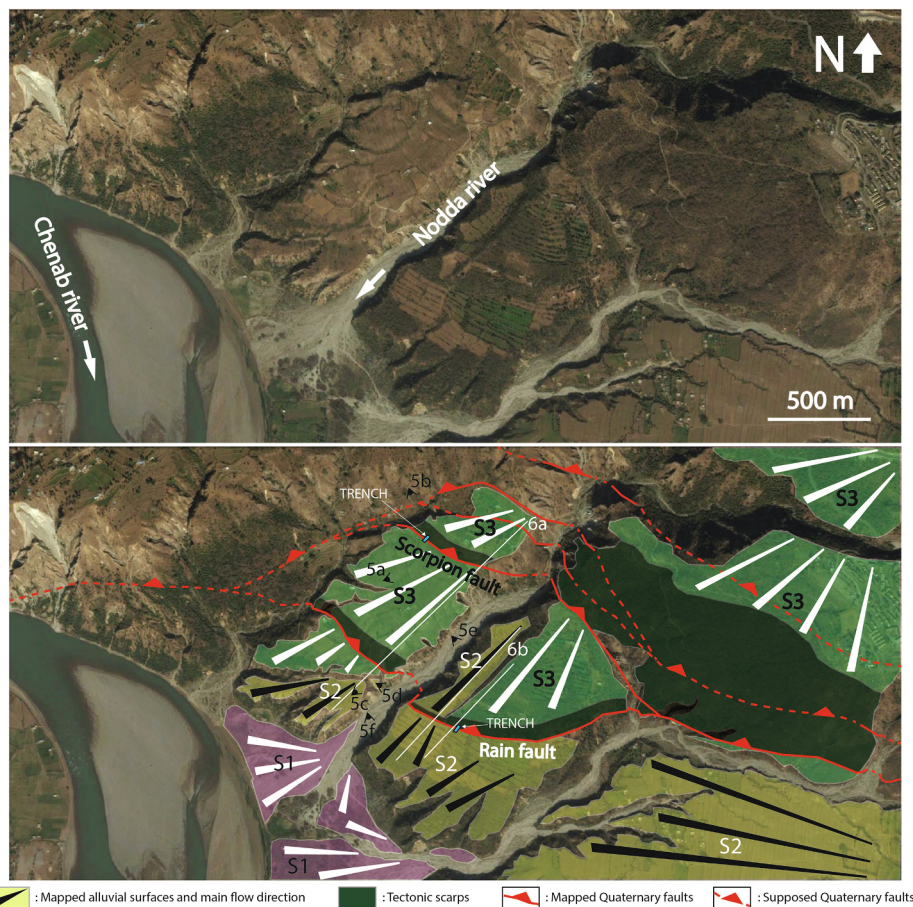


Fig. 3. Satellite image (Google Earth) of the Nodda river zone and mapping of the alluvial surfaces, tectonic scarps and fault branches. Pictures and topographic profiles presented in other figures are localized.

(Fig. 3). Vertical incision of the modern rivers carved canyons of more than 50 m deep and led to the abandonment of these alluvial surfaces. Present aggradation of the sediments at the outlet of these canyons builds new connected fans labeled S1. The abandoned alluvial fan system shows a hectometer-scale cumulated tectonic scarp along the MWT (Fig. 4). The scarp is located in a re-entrant of the MWT, where the fault trend bends from N 120°E on the eastern flank to N 70°E on the western flank (Figs. 1 and 2). Previous studies by Vassallo et al. (2015) and Mugnier et al. (2017) showed that scarp morphology has resulted from successive activity of several fault branches over a 2-km-wide fault zone, where the Precambrian limestones, belonging to the Lesser Himalaya unit, overthrust Siwalik conglomerates and Quaternary fan deposits on a 45°N dipping plane.

The morphology of the Nodda fan system (i.e. S2 and S3 surfaces, Figs. 3, 5a and c) and the shallow stratigraphy (Fig. 5b and 5d) indicate that Holocene fault activity is mainly concentrated on the two most external fault branches. These two branches are separated by about 500 m and are called respectively Scorpion and Rain faults (Figs. 3 and 4). These thrusts show ruptures reaching either the topographic surface or very shallow layers, and are associated with steep and sharp decameter-scale individual scarps (Figs. 3–5). The abrupt narrowing of the canyon width, from 70 m to 10 m upstream the trace of the Scorpion fault (Fig. 3), suggests a river incision response to differential uplift across this tectonic structure (Amos and Burbank, 2007; Yanites et al., 2010). The presence of large boulders of concrete material collapsed in the canyon at the toes of the Rain Fault offers evidence of localized and relatively recent weakening of the consolidated alluvial deposits along this structure. Displacements on more internal branches are sealed by undeformed deposits or by the planar morphology of the fan (Mugnier

et al., 2017). At Holocene time-scale, deformation is therefore migrating towards the frontal part of the Riasi thrust system.

In order to date and measure the latest stages in the deformation history, we focused on the tectonic record of the two decameter-scale Scorpion and Rain scarps. The two scarps, Scorpion (innermost) and Rain (outermost), are continuous over several kilometers, only interrupted by the recent vertical incision of the Nodda river within its own alluvial fan. (Fig. 3). The topographic slope in the steepest part of the scarps averages 30–35°, while in this zone the original slopes of the fan surface (surface S3) and of the inset terrace (surface S2) are ~4° and less than 3°, respectively. On the right bank, the surface vertical separation of S3 is 22 ± 2 m across the Scorpion scarp and 36 ± 3 m across the Rain scarp (Figs. 5a, c and 6a). On the left bank, the vertical surface separation across the Rain scarp are 26 ± 2 m (S3-S2) and 8 ± 1 m (S2-S2), respectively (Figs. 5d and 6b). The topographic profile along S2 shows a ~5 m counter-slope in the hanging-wall due to layers folding over the thrust ramp (Figs. 5e and 6b). This fold is likely due to a change in fault plane dip at shallow depth, as visible in the fault zone cross-section (Fig. 4b). We thus measured the surface vertical separation outside of the fold zone to minimize the effects of this local near-surface complexity on the vertical throw across the fault (see also Kaneda et al., 2008).

Stratigraphy of the alluvial fan and of the fill-and-cut terrace shows tabular up-ward fining sequences (40 cm–1 m thick) with planar bedding of clast-supported conglomerates (angular to sub-angular gravels to pebbles, well-sorted) alternating with sparse sand units (Vignoni et al., 2017). These sediments result from the mechanical erosion of the nearby steep hillslopes of Precambrian limestones, where Nodda river originates. The top stratigraphic units (over 30–50 cm) are slightly

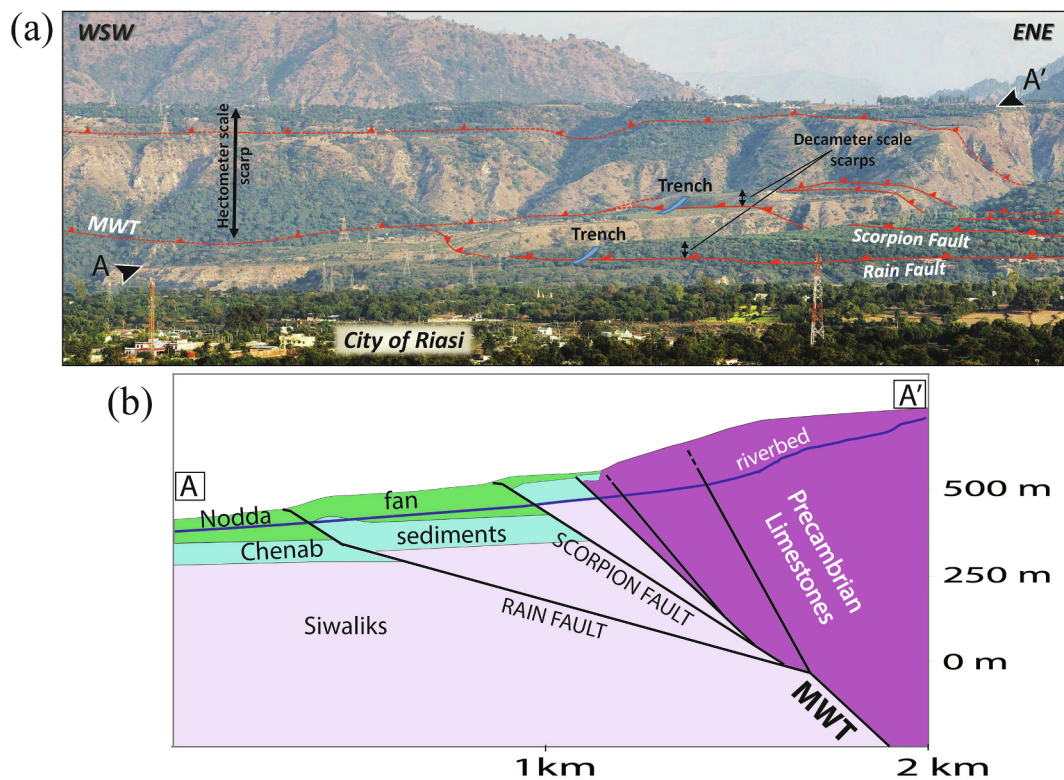


Fig. 4. (A) Panoramic view of the hectometer-scale tectonic scarp produced by MWT in the Riasi area. Within the alluvial fan of Nodda river, MWT split in several fault branches that are associated with decameter-scale scarps. The two outermost fault branches, the Scorpion Fault and the Rain Fault (in red), are the most active ones and the scarps associated with them show sharp morphologies. The trench sites are localized on these two fault branches; (B) Cross-section A-A' of the scarp showing the main fault branches (modified after Vassallo et al., 2015). (For interpretation of the references to colour in this figure legend, the reader is referred to the web version of this article.)

disturbed by human activity, as they are used to build cereal crops on terraces.

Above the fault branches associated with the decameter-scale scarps, alluvial layers are folded with a hectometer-scale wavelength. These layers dip gently northward in the back part of the folds (Fig. 5e) and they dip strongly southward in the fore part of the folds close to the fault zone (up to 60°, Fig. 5d). In the upper and middle part of the scarps, the sedimentary deposits preserved by erosion are continuous and not faulted (Fig. 5b and d). The brittle deformation is concentrated within the lower part of the two scarps. We trenched through these parts of the scarps in order to identify, measure and date as many seismo-sedimentary horizons as possible (Fig. 7).

4. Paleoseismological trenches method

In this geological context, seismic events generate co-seismic slips of several meters along low angle reverse fault plans. The hanging-wall tips, constituted by poorly consolidated sedimentary units, collapse immediately after each earthquake. The collapsed sediments of the hanging-wall produce colluvial wedges that seal the newly formed co-seismic ruptures and are therefore coeval of them. Thus, we assume that earthquakes may be dated by colluvial wedge using ^{14}C method. Nevertheless, the dating concerns the organic matter contained in the colluvial wedges and not directly the deposit formation. Charcoals used to date colluvial wedges, i.e. most of our samples, formed before their final deposit and therefore their dating yield a maximum age for the colluvial wedge formation. As a consequence, colluvial wedges dated by charcoals, even though simultaneous of the earthquakes, yield maximum ages for their occurrence.

Fourteen samples of organic matter, charcoals and bulk organic layers, were collected for ^{14}C dating (Table 1). Age discrepancies within

a same sedimentary unit may be due whether to reworking of older sediments (charcoals) or to pedogenetic processes that mix soil parts at different decomposition stages (bulk organic layers). In the former case, older samples must be considered as containing “inherited” ^{14}C and therefore yield overestimated ages. This effect should however be rather limited considering that the transit time from the source is short, due to the small size (few kilometers square) and very steep slopes of the catchment. In the latter case, the interpretation of the dating depends on the hypothesis about the formation and evolution of the soil units.

Co-seismic slips are estimated, when possible, by direct measurement of the distance along the fault between the footwall and hangingwall cutoffs of a sedimentary unit. However, in this context, the absence of clear piercing points due to erosion or gravitational collapse of the hangingwall often prevent this kind of measurement. To propose possible paleo-seismic scenarios for each trench and to quantify co-seismic displacements, we realized palinspastic restorations based on balanced cross-section principles (Elliott, 1983), as suggested by Mc Calpin (1996). These restorations are based on an interactive process to check the consistency between the initial and final stages of the section, and on a deformation style adapted to the granular formations involved (e.g. Ménard, 1988).

Unlike classical restorations on consolidated sediments, the layer parallel shearing assumption (e.g. Endignoux and Mugnier, 1990) is not suitable in superficial sediments because, in similar environments, the bed-parallel shortening can be greater than 30% (Jayangondaperumal et al., 2013). In this study we chose to apply an anisopach folding style with internal deformation and preservation of the deposit volumes (i.e. surface areas within the cross-section parallel to the slip vector), as this deformation style is observed in numerous Himalayan trenches (e.g. Lavé et al., 2005; Kumar et al., 2006; Bollinger et al., 2014; Mishra

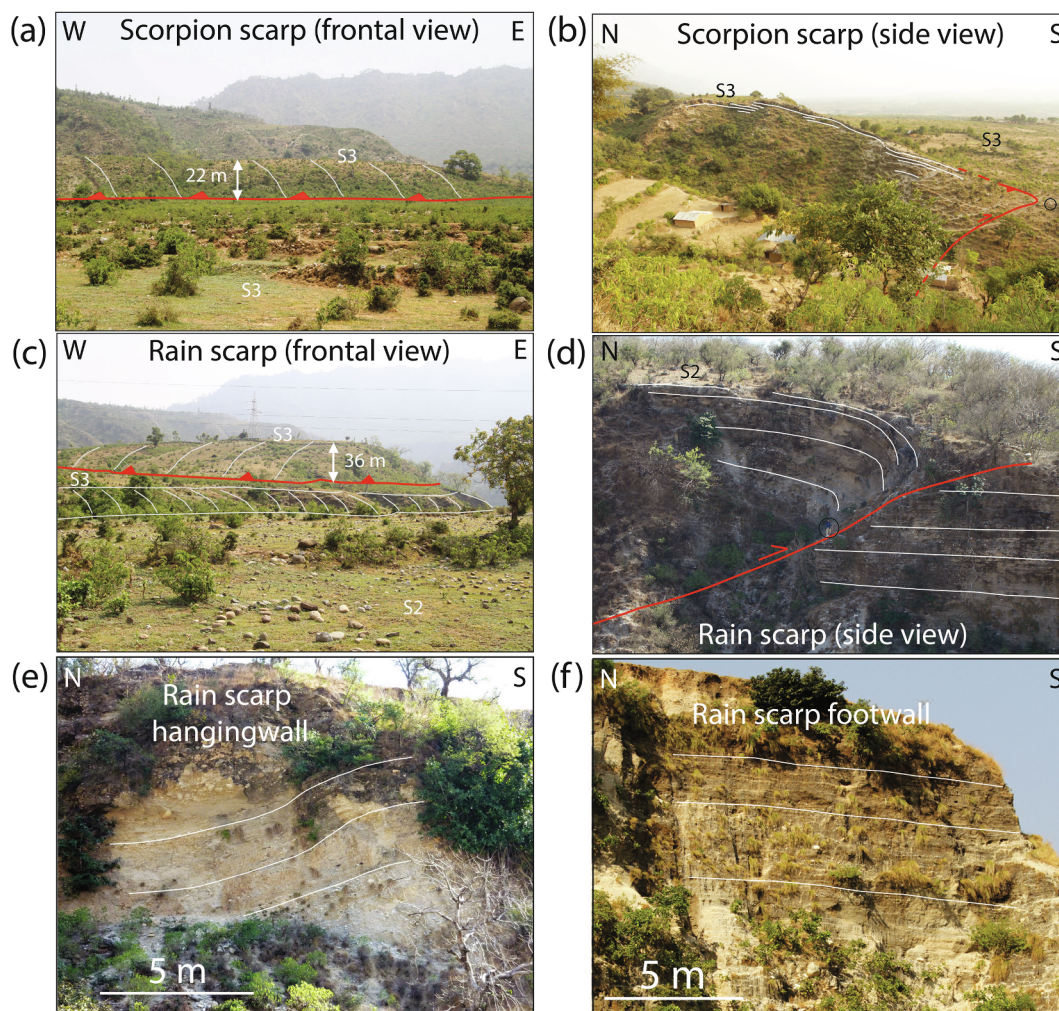


Fig. 5. Pictures of the decameter-scale scarps (localization in Fig. 3). White lines highlight the visible sedimentary layers, grey lines marks the topography in correspondence of the tectonic and alluvial scarps. (A) Scorpion scarp on the right bank of Nodda river seen from the foot-wall. Surface S3 is affected by a 22 ± 2 m vertical separation. Man-made terraces for cereal cultivation are visible in the foreground; (B) Scorpion scarp seen from the north-west through an oblique river incision. In the black circle, a person gives the scale. Continuous gravel beds preserved in the higher and middle part of the scarp indicate no significant brittle deformation reaching the surface within this part of the scarp; (C) Rain scarp on the right bank of Nodda river seen from the foot-wall. Surface S3 is affected by a 36 ± 3 m vertical separation and it is incised by surface S2 in the foot-wall; (D) Rain scarp across S2 on the left bank of Nodda river seen from the right bank. In the black circle, a person gives the scale. Surface S2 is affected by a 8 ± 1 m vertical separation. Gravel beds geometry shows folding in the hanging-wall and undeformed planar deposits in the foot-wall. Continuous beds at some distance from the main fault indicates that brittle deformation is concentrated in a few-meters-wide zone in the lower part of the scarp. The fault dips $\sim 15^\circ$ at surface and $\sim 30^\circ$ at the base of the canyon; (E) Folded layers at the back of the Rain scarp associated with a counter-slope at surface. This folding is determined by a change in fault plane dip at shallow depth; (F) Undeformed planar layers of the fan deposits, gently sloping toward the south-west.

et al., 2016; Le Roux-Mallouf et al., 2016). We must also take into account that volumes of these granular formations and fault rupture lengths can be lowered by compaction or by erosional episodes from one stage to another. Thus, for the restoration of a slip event, unit areas in the final stage may be either equivalent or smaller than in the initial stage. Such models are not meant to be unique, but the constraints given by the units' geometry/sedimentology and by the geochronological data minimize the plausible solutions.

5. Scorpion fault trench

5.1. Trench analysis

The trench across the Scorpion scarp was opened on the right bank of the Nodda river, where the Scorpion fault created a vertical surface separation of ~ 22 m across the pristine fan surface S3 (Figs. 3–5a and b). On this bank, the scarp has a steep slope – up to $30\text{--}35^\circ$ – and presents a sharp slope break at its base. The trench is 25 m long, 5 m

wide, and up to 8 m deep. Its direction is $N20^\circ E$, perpendicular to the fault branch. We chose to analyze in detail the eastern wall because the ruptures were better exposed and the samples suitable for dating more numerous (Figs. 7a and S1, available in the electronic supplement to this article). Three charcoals and five bulk organic samples were collected (Table 1).

Two main rupture zones (SF1 and SF2) perturb the stratigraphy succession of the fan, which can be divided into 7 sedimentary units called units S10–S70 (Fig. 7a). The innermost rupture (SF1) dips only few degrees to the north. Above the fault plane, in a stratigraphic order, we observe a first unit with planar cross-bedded structures of well-sorted pebbles and gravels, containing a 20-cm-thick silty layer, constituting the undeformed fan deposit (unit S10). Above this first unit, there is a large unconformable second unit of unsorted/locally sorted pebbles and gravels in a silty matrix that we interpret as a colluvial deposit (S20). Below the fault plane, unit S10 is recognizable by the same stratigraphy and by the silty layer described in the hanging-wall; a gravel deposit at the footwall of the fault SF1 may correspond to the

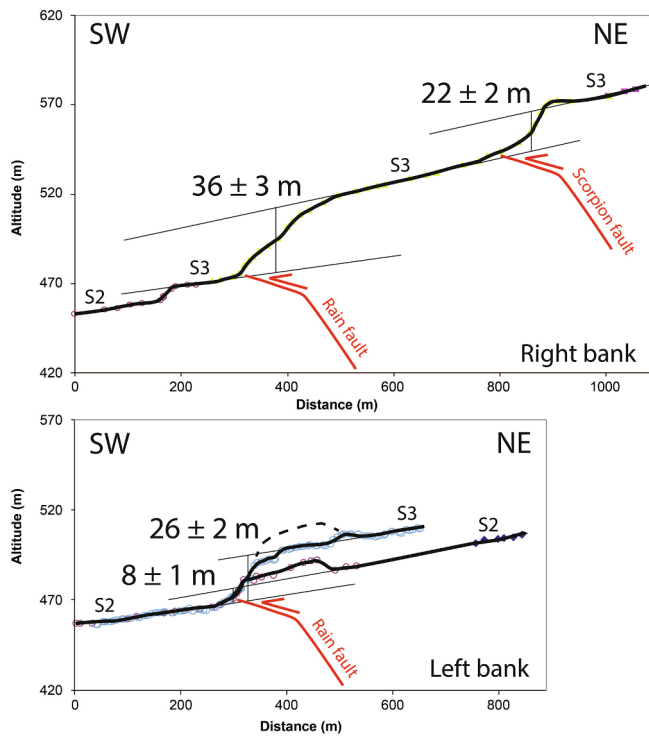


Fig. 6. Topographic profiles across the two scarps, on both banks of Nodda river (localization in Fig. 3), realized using total station and differential GPS surveys. Scarp heights across surfaces S2 and S3 are indicated. The dotted line represents the eroded pristine surface of S3.

lower part of unit S20. Unit S10 and supposed unit S20 are covered by an unconformable clay-rich unit (S30) with few sparse pebbles typical of a mud-flow deposit (Reineck and Singh, 1980). Hanging-wall and foot-wall units are both sealed by a large colluvial deposit rich in gravels and pebbles (S40). Another pebble-rich colluvial deposit (S60) lies unconformably over units S20 and S40.

The outermost rupture (SF2) is constituted by two main sub-parallel segments that dip 15°N and displace by 0.8 ± 0.2 m several gravel and sand beds from the fan deposit (S10). Two vertical sand dykes, resulting from liquefaction features that formed during a previous earthquake, are offset by the same amount. This rupture is sealed by a colluvial unit (S50), composed of poorly sorted gravel-rich material. This wedge lies unconformably over units S10 and S40. These three units, around the fault zone, are finally truncated by an erosion surface and overlaid by a soil with clustered pebbles zones (S70), which is of anthropic origin.

Colluvial unit S20 was dated by a bulk soil sample at 15155–14599 Cal BC (K12-17). Mud-flow unit S30 was dated at 4300 ± 200 Cal BC by the quasi-identical ages of a charcoal (K12-5) and of a bulk soil sample (K12-16). Colluvial unit S40 contains two charcoals dated at 1509–2278 Cal BC (K12-12 and K12-13) and an organic layer within the same age range (K12-18). The youngest charcoal yields the maximum age of this unit at 1661 Cal BC. Colluvial unit S50 does not contain organic material and cannot be directly dated. However, it lays over a small paleosol that was dated by a bulk sample at 1118–929 Cal BC (K12-20). Colluvial unit S60 was dated by a bulk organic sample at 850 ± 50 Cal BC (K12-22).

5.2. Restoration of Scorpion fault history

Fig. 8 shows the best palinspastic restoration for the main stages of the Scorpion scarp history. The oldest colluvial wedge within the trench (unit S20) formed around 14500–15000 BC (stage 1). No visible rupture is associated with the formation of this deposit, therefore its seismic origin is questionable. Later on, during several thousand years, this wedge has been partially eroded and finally buried by a mud-flow deposit (S30) at ~4300 BC (stage 2). After another erosional period (stage 3), the series was all faulted between 1661 BC and 929 BC by rupture SF1. This rupture triggered the collapse of the scarp, producing colluvial wedge unit S40 (stages 4 and 5). The apparent displacement for this event is estimated at 4.0 ± 1.0 m from our restoration.

The latest seismic event within the trench is associated with SF2 rupture. This event is responsible of a co-seismic slip of ~80 cm and induced a collapse of the hanging-wall tip that formed colluvial wedge unit S50 (stages 6 and 7). If we consider that organic activity in the paleosol below unit S50 stopped when the co-seismic collapse of the scarp buried it, its age of 1118–929 Cal BC corresponds to the age of the earthquake. This age is close to that of colluvial unit S60 in the upper part of the trench. This colluvial wedge possibly formed during the same earthquake or earthquakes sequence by the collapse of the steepest part of the scarp located above the trench.

6. Rain fault trench

6.1. Trench analysis

The trench across the Rain scarp was opened on the left bank of the Nodda river, where the S3 deposits thrust the S2 deposits (Figs. 3 and 4). At this place, the tectonic scarp is associated with a vertical surface separation of ~26 m and presents a steep morphology up to ~30° that trends N100°E. The trench is 16 m long, 5 m wide, up to 6 m deep, and is oriented N20°E. For the same reasons as for the Scorpion trench, we

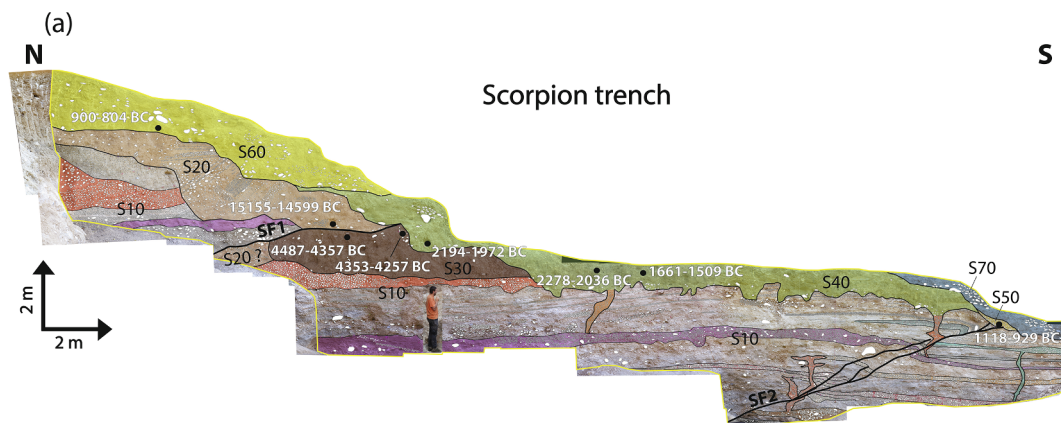


Fig. 7. Mosaic views of the eastern walls of the two trenches across the Scorpion fault branch (A) and the Rain fault branch (B) with interpretative logs and sample positions (sample marked by asterisk is situated on the western wall). For sedimentary units and ruptures description see the text. Details on ¹⁴C samples are given in Table 1 (all the ages are calibrated).

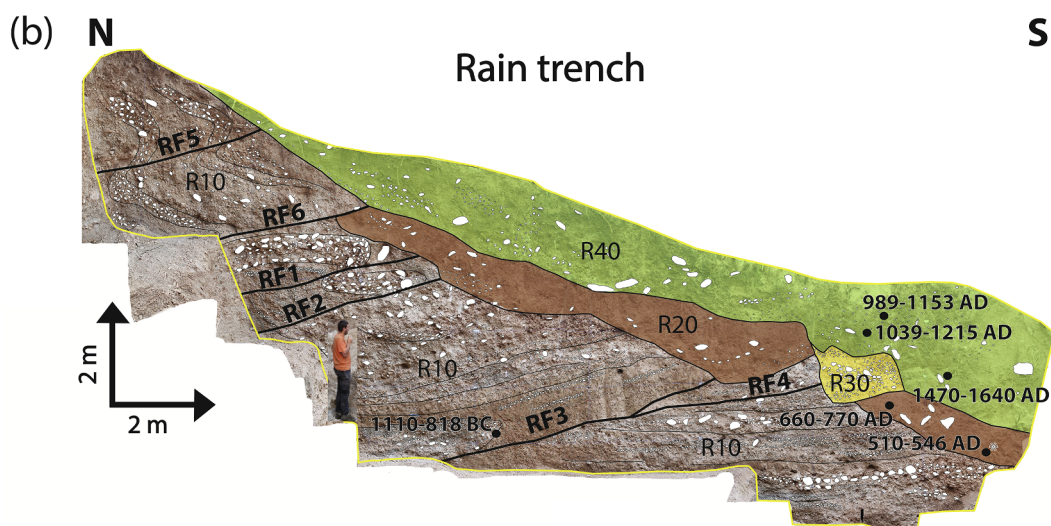


Fig. 7. (continued)

chose to analyze in detail the eastern wall (Figs. 7b and S2, available in the electronic supplement to this article). Five charcoals on this wall and one on the western wall were collected for ^{14}C dating (Table 1).

We observed six main ruptures (RF1 to RF6) and 4 sedimentary units called units R10 to R40. All ruptures affect unit R10, whose deposits are associated with the cut-and-fill terrace S2. Unit 10 is composed by quite well-sorted gravels to pebbles planar cross-bedded unit with fine sand and silty layers. All the ruptures are truncated and sealed by younger sedimentary units (R20 to R40), which allow determining a relative chronology among them.

Ruptures RF1, RF2 and RF3 are sealed by unit R20, which corresponds to a clay-rich mud-flow deposit. Rupture RF4, mainly overlapping with RF3, is sealed by unit R30, which corresponds to a colluvial wedge rich in gravels and pebbles. Above ruptures RF3-RF4, beds of unit R10 dip in average 15° to the north. These deposits initially dipped gently to the south-west, which suggests that they were tilted above a flat/ramp transition located along this rupture zone. We also observe a meter-scale drag fold above this rupture zone. Ruptures RF5 and RF6 are sealed by unit R40, which corresponds to another colluvial wedge mainly constituted by silty material and unsorted pebbles.

Unit R10 is dated at 1110–818 Cal BC by a charcoal (DAG C15). This ^{14}C age is close to the abandonment age of terrace S2 at ~ 3.8 ka (Vignon et al., 2017). Unit R20 contains two charcoals, DAG C14 and C4, the latter sampled on the western wall. They were dated respectively at 660–770 Cal AD and 510–546 Cal AD. We then consider a maximum age of 660 AD for the formation of this unit. Colluvial wedge

unit R30 does not contain organic matter and cannot be directly dated. Colluvial wedge unit R40 contains three charcoals in its lower part. They have ages spanning the period between 1000 and 1200 Cal AD (DAG C9 and DAG C10) to 1470–1640 Cal AD (DAG C12). The youngest charcoal yields the maximum age of the deposit, which therefore formed after 1470 AD.

6.2. Restoration of Rain fault history

Fig. 9 shows the best palinspastic restoration for the main stages of the Rain scarp history. To explain the present stratigraphy, the deposits of unit R10 have been firstly deformed creating a scarp in terrace S2 (stage 1 on Fig. 9). Then ruptures RF1 and RF2 occurred in the period comprised between 1110 BC and 660 AD, since they affect unit R10 and are sealed by unit R20 (stage 2). We can estimate ~ 1 m of co-seismic offset on RF1 and a minimum of 3 m on RF2, for which there is no piercing points. Rupture RF3 occurred during the same period (stage 3), possibly at the same time of ruptures RF1 and RF2. However, because of the geometry of the three ruptures, if they had occurred together it would imply a very large co-seismic slip. Considering uniquely the slip on RF3, we determine a minimum co-seismic slip of 5 ± 1.0 m.

The deposit of mud-flow unit R20 eroded the shallowest part of the three ruptures and sealed them after 660 AD (stage 4). Rupture RF4 re-activated part of RF3 segment and split in another segment toward the surface, creating a pebble-rich colluvial wedge (R30) by hanging-wall tip collapse (stages 5 and 6). This event occurred before the deposit of

Table 1

Results of the ^{14}C analysis. Samples were prepared and dated at CEA Saclay, Gif-sur-Yvette (France) and Poznan Radiocarbon Laboratory (Poland). Ages were calibrated using program OxCal v.4.2.4 (Bronk Ramsey and Lee, 2013) and the 2013 Northern Hemisphere calibration curve (Reimer et al., 2013).

Trench	Sample number	Lab code	Location	Type	^{14}C ages (BP)	Cal BC–AD (95.4%)
Scorpion	K12-5	SacA 31874	33°6.777'N 74°49.228'E	Charcoal	5455 \pm 30	4353–4257 Cal BC
Scorpion	K12-12	SacA 31878	33°6.777'N 74°49.228'E	Charcoal	3310 \pm 30	1661–1509 Cal BC
Scorpion	K12-13	SacA 31879	33°6.777'N 74°49.228'E	Charcoal	3745 \pm 30	2278–2036 Cal BC
Scorpion	K12-16	SacA 31,881	33°6.777'N 74°49.228'E	Bulk soil	5595 \pm 30	4487–4357 Cal BC
Scorpion	K12-17	SacA 31882	33°6.777'N 74°49.228'E	Bulk soil	13900 \pm 70	15155–14599 Cal BC
Scorpion	K12-18	SacA 31883	33°6.777'N 74°49.228'E	Bulk soil	3685 \pm 30	2194–1972 Cal BC
Scorpion	K12-20	SacA 31884	33°6.777'N 74°49.228'E	Bulk soil	2860 \pm 30	1118–929 Cal BC
Scorpion	K12-22	SacA 31885	33°6.777'N 74°49.228'E	Bulk soil	2690 \pm 30	900–804 Cal BC
Rain	Dag C4	Poz-40712	33°6.376'N 74°49.296'E	Charcoal	1580 \pm 30	510–546 Cal AD
Rain	Dag C9	Poz-40714	33°6.376'N 74°49.296'E	Charcoal	895 \pm 30	1039–1215 Cal AD
Rain	Dag C15	Poz-40715	33°6.376'N 74°49.296'E	Charcoal	2790 \pm 60	1110–818 Cal BC
Rain	Dag C12	Poz-40716	33°6.376'N 74°49.296'E	Charcoal	340 \pm 30	1470–1640 Cal AD
Rain	Dag C10	Poz-40718	33°6.376'N 74°49.296'E	Charcoal	990 \pm 30	989–1153 Cal AD
Rain	Dag C14	Poz-40719	33°6.376'N 74°49.296'E	Charcoal	1300 \pm 30	660–770 Cal AD

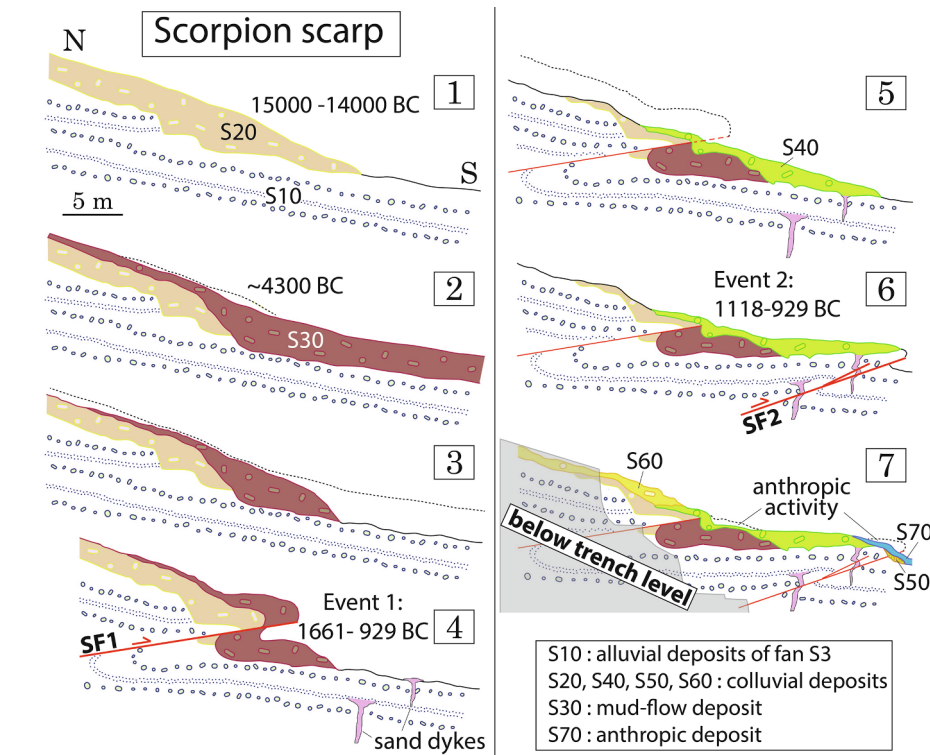


Fig. 8. Palinspastic restoration for the paleoseismic history across the Scorpion fault branch. Two ruptures occurred during the last ~3500 years. The first event occurred between 1661 and 929 BC, the second event occurred between 1118 and 929 BC.

the large colluvial wedge unit R40, which formed after 1470 AD. The co-seismic slip associated with this rupture is 1.0 ± 0.3 m.

The latest deformation event observed in the trench is associated with ruptures RF5 and RF6. Both of them are sealed by unit R40 and are therefore compatible with a single earthquake. Rupture RF6 makes unit R10 thrust above unit R20. The bending of pebble layers by rupture RF5 allows us measuring a slip of ~50 cm on this segment and our restoration yields a minimum slip of 3.0 ± 1.0 m along rupture RF6 (stages 7 and 8). This event produced a large colluvial wedge (R40), lying above these ruptures and previous deposits (R10, R20 and R30). The age of the colluvial wedge formation (post-1470 AD) and its large size are compatible with a main earthquake occurred on this thrust within the last five centuries.

7. Discussion

7.1. Paleoseismic calendar and 1555 AD Kashmir earthquake

Our present study attests for seismogenic deformation along the MWT during the Holocene in the Riasi area. Co-seismic primary ruptures reach the surface on two main fault branches at the toes of the km-scale tectonic scarp. Most of these ruptures are associated with co-seismic slips of several meters, instant collapse of the hanging-wall tip and formation of colluvial wedges. In this context, we consider that colluvial wedges are coeval with their respective seismic ruptures and we try to match our chronological findings with historical archives.

We found evidences for at least two seismic events along the Scorpion fault branch and for at least three seismic events along the Rain fault branch over the last ~3500 years. The oldest earthquake occurred between 1661 BC and 929 BC along the Scorpion fault and was characterized by several meters of co-seismic slip and a large colluvial wedge. A Persian historical account, the *Tarikh-e-Hasan* from Pir Hasan Shah (19th century AD), reports about a devastating earthquake around 1250 BC that affected the north of Kashmir basin (Iyengar et al., 1999). It is the oldest seismic event described in the historical literature

and its date is compatible with the age range of the oldest Scorpion rupture.

Then, Scorpion fault branch ruptured between 1118 BC and 929 BC with a co-seismic slip < 1 m. Rain fault branch ruptured at least once, more likely twice, between 1110 BC and 660 AD. It is thus possible that both fault branches ruptured together around 1000 BC. Unfortunately, there is no historical report in Kashmir area during this period for matching geological record with human testimony.

The penultimate event occurred along the Rain fault between 660 AD and 1470 AD. For this period, Persian and Sanskrit historical archives report of major earthquakes in 844 AD and 1123 AD felt in the Kashmir basin (Iyengar et al., 1999; Ahmad et al., 2009). Given the lack of information about the location and the extent of damage, both of them may correspond to this record or be associated with other Kashmir fault systems.

The latest event, formally dated as post-1470 AD along the Rain fault branch (ruptures RF5 and RF6), is associated to one of the largest colluvial wedges observed (R40), suggesting that its triggering was due to a particularly strong shaking. The 1555 AD earthquake, the main event historically recorded during this period, was strongly felt in the whole Kashmir Basin and the main damaged areas were respectively at 50 km to the south-west and at 140 km to the south-east of Srinagar (Iyengar et al., 1999; Ambraseys and Jackson, 2003). These places are both located in the hanging-wall of MWT at the vicinity of the fault emergence. The colluvial wedge dating and size combined with the historical localization of damages in Kashmir region with respect to the MWT trace make the great Kashmir earthquake of 1555 AD to be the best candidate for this rupture.

7.2. Co-seismic slips in the Himalayan context

Since co-seismic slips are large, part of the recorded deformation is systematically lost in the gravitational collapse of the hanging-wall and clear piercing points along the ruptures are often absent. In this context, palinspastic restorations are fundamental to complete direct

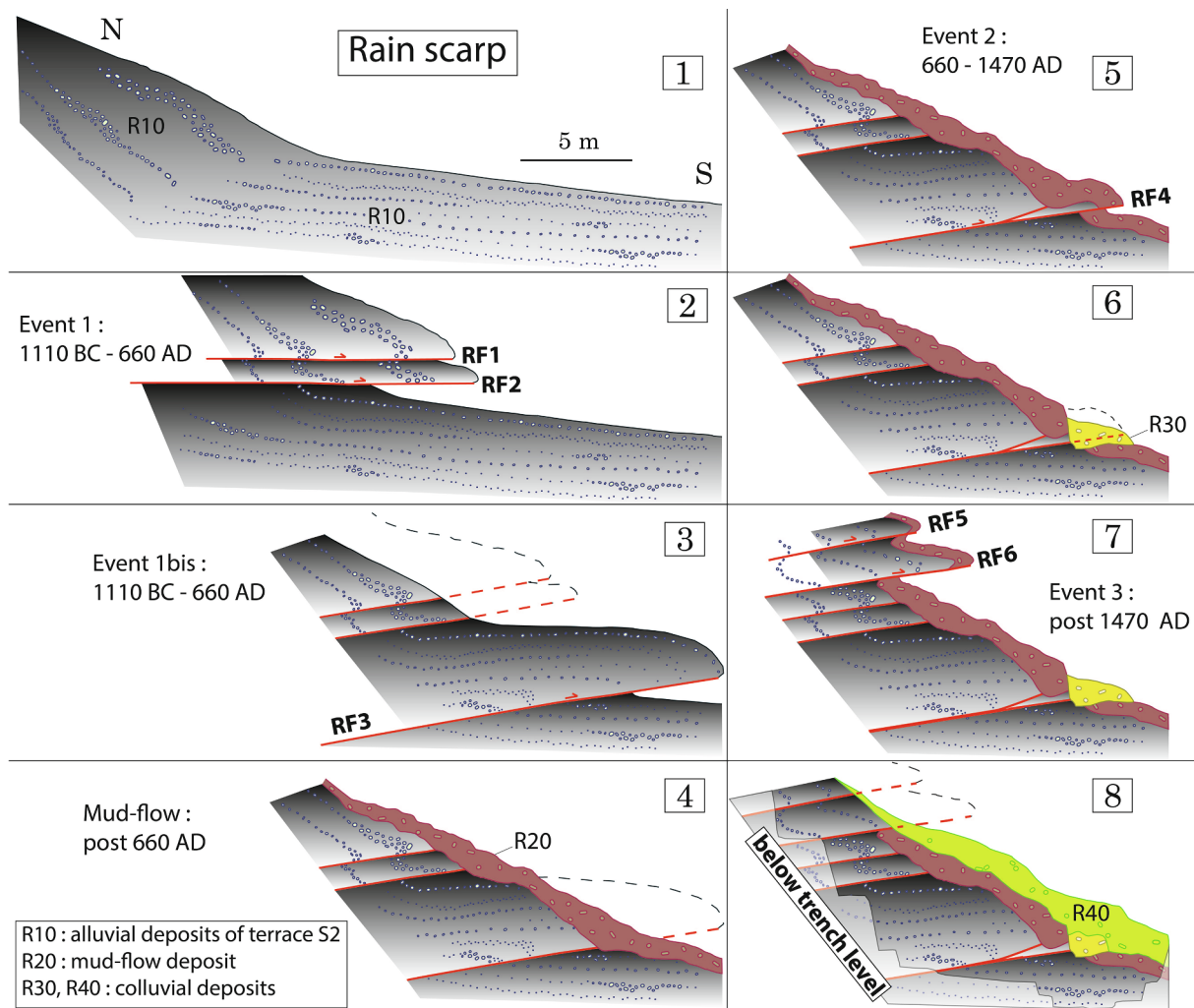


Fig. 9. Palinspastic restoration for the paleoseismic history across the Rain fault branch. At least three ruptures occurred during the last ~3100 years. The first event, which may be the sum of two distinct ruptures, occurred between 1110 BC and 660 AD. The second event occurred between 660 and 1470 AD. The latest event occurred after 1470 AD.

measurements and be able to determine slip estimates. Using this method, we found that co-seismic slips for each event may vary from less than 1 m to more than 5 m.

However, co-seismic slips at surface along Himalayan thrusts are not always directly linked to earthquakes magnitude. Indeed, the main seismogenic décollement at the base of the Himalayan range gently dips to the north, with the consequence that the distance between the epicenters and the frontal ramps may vary from few km to more than a hundred km (Mugnier et al., 2013; Schiffman et al., 2013; Kundu et al., 2014). It is particularly evident considering the latest earthquakes: the 2015 Mw 7.8 Gorkha earthquake, triggered on the main detachment, did not even produce primary surface ruptures (e.g. Avouac et al., 2015; Grandin et al., 2015; Kobayashi et al., 2015) whereas the 2005 Mw 7.6 Balakhot-Bagh earthquake, triggered at the base of the ramp, produced surface ruptures with slips up to 7 m (Kaneda et al., 2008). Thus, co-seismic slips of 1 m or less observed in the Riasi trenches may correspond either to relatively small or medium ($M_w < 7.5$) events triggered in the vicinity of the emergence of the MWT at surface or to big ($M_w > 7.5$) events triggered tens of kilometers northward on the main detachment.

Moreover, the amplitude of co-seismic slip at surface may be biased by diffusive component of the deformation. This phenomenon is likely enhanced by the rheology of thick Quaternary sedimentary cover composed by weakly or partially consolidated granular material. When

alluvial deposits thickness is particularly important – several tens or hundreds of meters – surface ruptures may even locally die out along the fault trace, as observed within most of the fill terraces crossing the fault in the near Pakistan Kashmir during the 2005 Balakhot-Bagh earthquake (Kaneda et al., 2008). The lack of morphological expression of faulting in these contexts suggests that deformation could be absorbed at small scale (from microscopic to clast scale), for example by grains rotation and dilatancy during shaking events (Iwashita and Oda, 2000).

In the Riasi area, diffusive deformation in granular material occurs with another type of non-localized deformation undetectable in paleoseismological trenches, which is the hectometer-scale folding of alluvial deposits. This kind of deformation is particularly clear looking at the geometry of topography and stratigraphy of terrace S2 in the hanging-wall of the Rain fault (Figs. 5 and 6). The surface uplift due to folding locally adds to the surface uplift due to the vertical slip on the fault plane. This phenomenon partly explain how tectonic scarps more than 20 m high are built over gently-dipping fault branches in a few thousand years.

8. Conclusion

In Kashmir Himalaya, we determined the chronology and the spatial pattern of the latest five seismic paleo-ruptures recorded within the

sediments stratigraphy of an alluvial fan along the Medlicott-Wadia Thrust. These ruptures are localized in the Riasi area, at the front of a main hectometer-scale tectonic scarp where two distinct fault branches are associated with decameter-scale scarps. Paleoseismic events recognized on these two fault branches are characterized by slips from < 1 m to > 5 m occurred between ~1500 BC and post-1470 AD, resulting in a mean recurrence interval of large seismic events along this section of the MWT between 500 and 700 years. Age and characteristics of the latest event are compatible with the great historical Kashmir earthquake of 1555 AD, implying that the occurrence of a major event in the next decades is probable.

CRedit authorship contribution statement

Riccardo Vassallo: Conceptualization, Methodology, Formal analysis, Investigation, Visualization, Supervision, Project administration. **Jean-Louis Mugnier:** Conceptualization, Methodology, Formal analysis, Investigation, Project administration. **Hervé Jomard:** Methodology, Formal analysis, Investigation, Visualization. **Joaquin Cortès Aranda:** Formal analysis, Visualization. **Manzoor A. Malik:** Supervision, Project administration. **François Jouanne:** Visualization. **Jean-François Buoncristiani:** Investigation.

Declaration of Competing Interest

The authors declare that they have no known competing financial interests or personal relationships that could have appeared to influence the work reported in this paper.

Acknowledgments

This study was funded by the PAKSIS program of the ANR Catel, CNRS/INSU TS-ALEAS program, and Labex@OSUG 2020. 14C ages were obtained by the INSU national service SMA Artemis at LMC14, Saclay, France. We thank R. Jayangondaperumal for the fruitful discussions. We acknowledge an anonymous reviewer and editor M. Pandit for their fruitful comments that helped to improve the manuscript. We thank Jammu and Kashmir inhabitants for their help in opening and cleaning the trenches and for their warm hospitality.

Appendix A. Supplementary material

Supplementary data to this article can be found online at <https://doi.org/10.1016/j.jseaes.2020.104505>.

References

- Ahmad, B., Bhat, M.I., Bali, B., 2009. Historical record of earthquakes in the Kashmir Valley. *Himal. Geol.* 30 (1), 75–84.
- Ahmad, S., Bhat, M.I., 2012. Tectonic geomorphology of the Rambhara basin, SW Kashmir Valley reveals emergent out-of-sequence active fault system. *Himal. Geol.* 33, 162–172.
- Ambraseys, N.N., Jackson, D., 2003. A note on early earthquakes in northern India and southern Tibet, Bangalore, INDE, Current Science Association, 13 p.
- Ambraseys, N.N., Douglas, J., 2004. Magnitude calibration of north Indian earthquakes. *Geophys. J. Int.* 159, 165–206.
- Amos, C.B., Burbank, D.W., 2007. Channel width response to differential uplift. *J. Geophys. Res.* 112, F02010. <https://doi.org/10.1029/2006JF000672>.
- Avouac, J.-P., Ayoub, F., Leprince, S., Konca, O., Helmberger, D.V., 2006. The 2005, Mw 7.6 Kashmir earthquake: Sub-pixel correlation of ASTER images and seismic waveforms analysis. *Earth Planet. Sci. Lett.* 249, 514–528.
- Avouac, J.-P., Meng, L., Wei, S., Wang, T., Ampuero, J.P., 2015. Lower edge of locked Main Himalayan Thrust unzipped by the 2015 Gorkha earthquake. *Nat. Geosci.* 8, 1752–1759.
- Bilham, R., 2001. Slow tilt reversal of the Lesser Himalaya between 1862 and 1992 at 78°E, and bounds to the southeast rupture of the 1905 Kangra earthquake. *Geophys. J. Int.* 144, 713–728.
- Bilham, R., 2019. Himalayan earthquakes: a review of historical seismicity and early 21st century slip potential. *Geol. Soc., Lond., Special Publ.* 483 (1), 423–482. <https://doi.org/10.1144/SP483.16>.
- Bollinger, L., Sapkota, S.N., Tapponnier, P., Klinger, Y., Rizza, M., Van Der Woerd, J., Tiwari, D.R., Pandey, R., Bitri, A., Bes de Berc, S., 2014. Estimating the return times of great Himalayan earthquakes in eastern Nepal: evidence from the Patu and Bardibas strands of the Main Frontal Thrust. *J. Geophys. Res.* 119, 7123–7163.
- Bronk Ramsey, C., Lee, S., 2013. Recent and Planned Developments of the Program OxCal. *Radiocarbon* 55 (2–3), 720–730.
- Burbank, D.W., Reynolds, R.G.H., Johnson, G.D., 1986. Late Cenozoic tectonics and sedimentation in the north-western Himalayan foredeep. In: *II: Eastern limb of the Northwest Syntaxis and regional synthesis v. 8*. Special Publication of the International Association of Sedimentologists, pp. 293–306.
- Dar, R.A., Romshoo, S.A., Chandra, R., Ahmad, I., 2014. Tectono-geomorphic study of the Karewa Basin of Kashmir Valley. *J. Asian Earth Sci.* 92, 143–156.
- Elliott, D., 1983. The construction of balanced cross-sections. *J. Struct. Geol.* 5 (2), 101.
- Endignoux, L., Mugnier, J.-L., 1990. The use of a forward kinematic model in the construction of balanced cross-section. *Tectonics* 9, 1249–1262.
- Gansser, A., 1964. *Geology of the Himalayas*: Inter Science Publishers, John Wiley & Sons, pp. 289.
- Gavillot, Y., Meigs, A., Yule, Y., Heennanoe, R., Ritoenour, T., Madugo, C., Malik, M., 2016. Shortening rate and Holocene surface rupture on the Riasi fault system in the Kashmir Himalaya: Active thrusting within the Northwest Himalayan orogenic wedge. *Geol. Soc. Am. Bull.* 128 (7–8), 107–1094. <https://doi.org/10.1130/831281.1>.
- Grandin, R., Vallée, M., Satriano, C., Lacassin, R., Klinger, Y., Simoes, M., Bollinger, L., 2015. Rupture process of the Mw = 7.9 Gorkha earthquake (Nepal): Insights into Himalayan megathrust segmentation. *Geophys. Res. Lett.* 42 (20), 8373–8382.
- Hebeler, A., Madden, C., Malik, M.A., Kaericher, M., Gavillot, Y., Yule, D., Meigs, A., 2010. Middle Holocene surface rupture of the Riasi thrust, Kashmir, India: Annual meeting of the Seismological Society of America, Portland, OR, 21–23 April.
- Jade, S., Mukul, M., Gaur, V.K., Kumar, K., Shringeshwar, T.S., Satyal, G.S., Dumka, R.K., Jagannathan, S., Ananda, M.B., Kumar, P.D., Banerjee, S., 2014. Contemporary deformation in the Kashmir-Himachal, Garhwal and Kumaon Himalaya: significant insights from 1995–2008 GPS time series. *J. Geod.* 88, 539–557. <https://doi.org/10.1007/s00190-014-0702-3>.
- Jayangondaperumal, R., Mugnier, J.L., Dubey, A.K., 2013. Earthquake slip estimation from the scarp geometry of Himalayan Frontal Thrust, western Himalaya: Implications for seismic hazard assessment. *Int. J. Earth Sci.* <https://doi.org/10.1007/s00531-013-0888-2>.
- Kaneda, H., Nakata, T., Tsutsumi, H., Kondo, H., Sugito, N., Awata, Y., Akhtar, S.S., Majid, A., Khattak, W., Awan, A.A., Yeats, R.S., Hussain, A., Ashraf, M., Wesnousky, S.G., Kausar, A.B., 2008. Surface rupture of the 2005 Kashmir, Pakistan, earthquake and its active tectonic implications. *Bull. Seismol. Soc. Am.* 98, 521–557.
- Kobayashi, T., Morishita, Y., Yurai, H., 2015. Detailed crustal deformation and fault rupture of the 2015 Gorkha earthquake, Nepal, revealed from ScansAR-based interferograms of ALOS-2. *Earth Planets Space* 67 (1), 1–13.
- Kondo, H., Nakata, T., Akhtar, S., Wesnousky, S., Sugito, N., Kaneda, H., Tsutsumi, H., Khan, A., Khattak, W., Kausar, A., 2008. Long recurrence interval of faulting beyond the 2005 Kashmir earthquake around the northwestern margin of the Indo-Asian collision zone. *Geology* 36, 731–734. <http://dx.doi.org/10.1130/G25028A>.
- Krishnaswamy, V.S., Jalote, S.P., and Shome, S.K., 1970. Recent crustal movements in north-west Himalaya and the Gangetic foredeep and related patterns of seismicity. In: *Symp. Earthquake Eng., 4th Roorkee*, pp. 419–439.
- Kumahara, Y., Nakata, T., 2006. Active Faults in the Epicentral Area of the 2005 Pakistan Earthquake. *Spec. Publ. Res. Cent. Reg. Geogr. Hiroshima Univ.*, v. 41, p. 54, CD.
- Kumar, S., Wesnousky, S.G., Rockwell, T.K., Briggs, R., Thakur, V.C., Jayangondaperumal, R., 2006. Paleoseismic evidence of great surface-rupture earthquakes along the Indian Himalaya. *J. Geophys. Res.* 111, B03304. <https://doi.org/10.1029/2004JB003309>.
- Kundu, B., Yadav, R.K., Bali, B.S., Chowdhury, S., Gahalaut, V.K., 2014. Oblique convergence and slip partitioning in the NW Himalaya: Implications from GPS measurements. *Tectonics* 33, 2013–2024. <https://doi.org/10.1002/2014TC003633>.
- Iwashita, K., Oda, M., 2000. Micro-deformation mechanism of shear banding process based on modified distinct element method. *Powder Technol.* 109, 192–205.
- Iyengar, R.N., Sharma, D., Siddiqui, J.M., 1999. Earthquake history of India in medieval times. *Indian J. Hist. Sci.* 34 (3), 181–237.
- Lavé, J., Yule, D., Sapkota, S., Basant, K., Madden, C., Attal, M., Pandey, R., 2005. Evidence for a great medieval earthquake (1100 A.D.) in the central Himalayas, Nepal. *Science* 307, 1302–1305. <https://doi.org/10.1126/science.1104804>.
- Le Roux-Mallouf, R., Ferry, M., Ritz, J.-F., Berthet, T., Cattin, R., Drukpa, D., 2016. First paleoseismic evidence for great surface-rupturing earthquakes in the Bhutan Himalayas. *J. Geophys. Res. Solid Earth* 121. <https://doi.org/10.1002/2015JB012733>.
- Mc Calpin, J., 1996. *Paleoseismology* 62 Academic Press International Geophysics Series 588 pages.
- Ménard, G., 1988. Méthodologie générale de construction des coupes équilibrées. In: *L'équilibre des coupes géologiques: buts, méthodes et applications* (Ed. par Gratier, J. P.) *Mém. et doc. C.A.E.S.S. (Rennes)* 20, 5–25.
- Mishra, R.L., Singh, A., Pandey, A.K., Rao, P.S., Sahoo, H.K., Jayangondaperumal, R., 2016. Paleoseismic evidence of a giant medieval earthquake in the eastern Himalaya. *Geophys. Res. Lett.* 43, 5707–5715. <https://doi.org/10.1002/2016GL068739>.
- Mugnier, J.L., Gajurel, A., Huyghe, P., Jayangondaperumal, R., Jouanne, F., Upreti, B., 2013. Structural interpretation of the great earthquakes of the last millennium in Central Himalaya. *Earth Sci. Rev.* 127, 30–47.
- Mugnier, J.-L., Vignon, V., Jayangondaperumal, R., Vassallo, R., Malik, M.A., Replumaz, A., Srivastava, R.P., Jouanne, F., Buoncristiani, J.F., Jomard, H., Carcaillet, J., 2017. A complex thrust sequence in western Himalaya: The active Medlicott Wadia Thrust. *Quat. Int.* <https://doi.org/10.1016/j.quaint.2017.05.028>.
- Nakata, T., Tsutsumi, H., Khan, S., Lawrence, R., 1991. Active Faults of Pakistan.

- Research Center for Regional Geography, Hiroshima University, Special publication N° 21 141 p.
- Pathier, E., Fielding, E.J., Wright, T.J., Walker, R., Parsons, B.E., Hensley, S., 2006. Displacement field and slip distribution on the 2005 Kashmir earthquake from SAR imagery. *Geophys. Res. Lett.* 33, L20310. <https://doi.org/10.1029/2006GL027193>.
- Powers, P.M., Lillie, R.J., Yeats, R.S., 1998. Structure and shortening of the Kangra and Dehra Dun reentrants, Sub-Himalaya, India. *Geol. Soc. Am. Bull.* 110, 1010–1027.
- Reimer, P.J., Bard, E., Bayliss, A., Beck, J.W., Blackwell, P.G., Bronk Ramsey, C., Grootes, P.M., Guilderson, T.P., Hafliðason, H., Hajdas, I., Hattž, C., Heaton, T.J., Hoffmann, D.L., Hogg, A.G., Hughen, K.A., Kaiser, K.F., Kromer, B., Manning, S.W., Niu, M., Reimer, R.W., Richards, D.A., Scott, E.M., Southon, J.R., Staff, R.A., Turney, C.S.M., van der Plicht, J., 2013. IntCal13 and Marine13 radiocarbon age calibration curves 0–50,000 years cal BP. *Radiocarbon* 55 (4).
- Reineck, H.E., Singh, I.B., 1980. *Depositional Sedimentary Environments with Reference to Terrigenous Clastics*. Springer Verlag, Berlin, pp. 549.
- Schiffman, C., Bali, B.S., Szeliga, W., Bilham, R., 2013. Seismic slip deficit in the Kashmir Himalaya from GPS observations. *Geophys. Res. Lett.* 40, 5642–5645. <https://doi.org/10.1002/2013GL057700>.
- Shah, A.A., 2013. Earthquake geology of Kashmir Basin and its implications for future large earthquakes. *Int. J. Earth Sci. (Geol. Rundsch)*. <https://doi.org/10.1007/s00531-013-0874-8>.
- Shah, A.A., 2015. Kashmir Basin Fault and its tectonic significance in NW Himalaya, Jammu and Kashmir, India. *Int. J. Earth Sci.* 104, 1901–1906.
- Shah, A.A., 2016. No major active backthrust bounds the Pir Panjal Range near Kashmir basin, NW Himalaya. *J. Asian Earth Sci.* <https://doi.org/10.1016/j.jseaes.2016.03.017>.
- Thakur, V.C., Jayangondaperumal, R., Malik, M.A., 2010. Redefining Medicott-Wadia's main boundary fault from Jhelum to Yamuna, An active fault strand of the main boundary thrust in northwest Himalaya. *Tectonophysics* 489, 29–42.
- Vassallo, R., Mugnier, J.-L., Vignon, V., Malik, M.A., Jayangondaperumal, R., Srivastava, P., Jouanne, F., Carcaillet, J., 2015. Distribution of the Late-Quaternary deformation in Northwestern Himalaya, Earth and Planetary Sci. Lett. 411, 241–252. <https://doi.org/10.1016/j.epsl.2014.11.030>.
- Vignon, V., 2011. *Activité hors séquence des chevauchements dans la syntaxe nord-ouest himalayenne: apports de la modélisation analogique et quantification quaternaire par analyse morphotectonique*. PhD thesis. Université de Grenoble, France, 278 p.
- Vignon, V., Mugnier, J.-L., Vassallo, R., Srivastava, P., Malik, M.A., Jayangondaperumal, R., Jouanne, F., Buoncristiani, J.-F., Carcaillet, J., Replumaz, A., Jomard, H., 2017. Sedimentation close to the active Medicott Wadia Thrust (Western Himalaya): How to estimate climatic base level changes and tectonics. *Geomorphology* 284, 175–190. <https://doi.org/10.1016/j.geomorph.2016.07.040>.
- Wallace, K., Bilham, R., Blume, F., Gaur, V.K., Gahalaut, V., 2005. Surface deformation in the region of the 1905 Kangra Mw = 7.8 earthquake in the period 1846–2001. *Geophys. Res. Lett.* 32, L15307. <https://doi.org/10.1029/2005GL022906>.
- Yan, Y., Pinel, V., Trouvé, E., Pathier, E., Perrin, J., Bascou, P., Jouanne, F., 2013. Coseismic slip distribution of the 2005 Kashmir earthquake from SAR amplitude image correlation and differential interferometry. *Geophys. J. Int.* <https://doi.org/10.1093/gji/ggs102>.
- Yanites, B.J., Tucker, G.E., Mueller, K.J., Chen, Y., 2010. How rivers react to large earthquakes: Evidence from central Taiwan. *Geology* 38 (7), 639–642. <https://doi.org/10.1130/G30883.1>.